Int J Civ Eng (2016) 14:507–519
DOI 10.1007/s40999-016-0024-3

RESEARCH PAPER

Nonlinear Finite Element Modeling of Shear-Critical Reinforced Concrete Beams Using a Set of Interactive Constitutive Laws

Vahid Broujerdian[1] · **Mohammad Taghi Kazemi**[2]

Received: 12 April 2015 / Revised: 12 October 2015 / Accepted: 16 April 2016 / Published online: 25 May 2016

Abstract Complex nature of diagonal tension accompanied by the formation of new cracks as well as closing and propagating preexisting cracks has deterred researchers to achieve an analytical and mathematical procedure for accurate predicting shear behavior of reinforced concrete, and there is the lack of a unique theory accepted universally. Shear behavior of reinforced concrete is studied in this paper based on recently developed constitutive laws for normal strength concrete and mild steel bars using the nonlinear finite element method. The salient feature of these stress–strain relations is to account the interactive effects of concrete and embedded bars on each other in a smeared rotating crack approach. Implementing the considered constitutive laws into an efficient secant-stiffness-based finite element algorithm, a procedure for the nonlinear analysis of reinforced concrete is achieved. The resulted procedure is capable of predicting load-deformation behavior, cracking pattern, and failure mode of reinforced concrete. Corroboration with data from shear-critical beam test specimens with a wide range of properties showed the model to predict responses with a good accuracy. The results were also compared with those from the well-known theory of modified compression field and its extension called disturbed stress field model which revealed the present study to provide more accurate predictions.

✉ Vahid Broujerdian
broujerdian@iust.ac.ir

[1] Iran University of Science and Technology, Tehran, P.O. Box 16765-163, Iran

[2] Sharif University of Technology, Tehran, P.O. Box 11365-9313, Iran

Keywords Reinforced concrete · Interactive constitutive laws · Smeared crack model · Finite element model · Load-deformation response · Shear-critical beams

1 Introduction

Predicting load-deformation behavior, cracking pattern, strength, and stiffness of shear-critical reinforced concrete (RC) members has been the focus of a lot of research over the last century [1, 2]. However, complex nature of diagonal tension accompanied by the formation of new cracks as well as closing and propagating preexisting cracks has deterred researchers to achieve an analytical and mathematical solution.

A part of the literature in this field contains the studies aimed to obtain cracking shear strength or ultimate shear strength of RC structural elements regardless their complete load-deformation response. These studies are usually based upon simplified physical models—considering classical mechanics of material [3–11] or fracture mechanics [12–16] and experimental data fitting. Therefore, each of these models is applicable for a certain range of specifications that they crystalized and calibrated for. Another part of the literature contains the studies aimed to achieve full load-deformation response of reinforced concrete in a general 2D or 3D loading condition. To achieve such response, one needs to consider constitutive, equilibrium, and compatibility equations, simultaneously. These studies can be divided into smeared crack and discrete crack approaches. The former category models the cracks by applying an equivalent theory of continuum mechanics and assumes the cracks as rotating or fixed [17–31]. The difference of these procedures is mainly due to, first, the different constitutive laws they adopted, and second, the

numerical approach that they used to solve the aforementioned equations. The latter category is based on fracture mechanics principles and models the cracks as geometric discontinuities [32–36].

This paper reports the second part of a study aiming to capture the full load-deformation response of RC beams. In the first part, a set of constitutive laws for normal strength concrete and embedded steel bars was developed to predict the response of cracked reinforced concrete subjected to in-plane stresses [28]. An interesting property of these stress–strain relations is to account the interactive effects of concrete and embedded bars on each other. In this model, the amount of reinforcement ratio is supposed to affect average stress–strain relation of cracked concrete in tension and compression. On the other hand, the model accounts for the effect of concrete on the average behavior of reinforcing bars. This model is categorized as an orthotropic smeared rotating crack model. Orthotropic models present uniaxial stress–strain relations in the axes of orthotropy.

The aim of this paper is to implement the aforementioned constitutive laws into finite element method, FEM, and to validate the model with experimental data. The numerical algorithm used here is based on the procedure proposed by Vecchio [19] and it is an iterative, secant-stiffness formulation. Simplicity of implementing due to applying some modifications on linear FEM and possibility of using low-order elements is two salient characteristics of this approach.

To assess the robustness of the proposed method, it is implemented on several reinforced concrete shear-critical beams. The results are corroborated with the experimental data. In addition, for the sake of comparison, the results of modified compression field theory, MCFT, [18, 19] and its extension disturbed stress field model, DSFM, [20–22] are included in the paper. It is observed from the results that the proposed approach provides load-deformation behavior, cracking pattern, and failure mode prediction with an excellent agreement with the experimental data; furthermore, it has more accuracy than MCFT and DSFM. More interestingly, in beams containing no transverse reinforcement and subjected to a high shear span-to-depth ratio in which MCFT, DSFM, and other prevailing methods show a considerable deficiency, the present study provides good predictions.

2 Materials and Methods

2.1 Constitutive Laws

The basic information needed for analyzing every structure is stress–strain relations under various conditions of loading, and reinforced concrete structures are not exceptional. In this paper, the stress–strain relations proposed in a recent research [28] are utilized for nonlinear finite element modeling of reinforced concrete beams. This approach is based on smeared crack concept, and it is an orthotropic model which considers different uniaxial stress–strain relations in the axes of orthotropy. In what follows, a detailed description of compressive and tensile stress–strain relation is presented.

2.1.1 Average Stress–Strain Relationship of Steel

Since it is assumed in many studies that reinforcing bars can only transmit axial forces, a bilinear uniaxial stress–strain relationship, as shown in Fig. 1a, is adopted to model the behavior of embedded reinforcing steels in the concrete. However, the behavior of an embedded bar in concrete is different from a bare one. When a crack initiates, the concrete fails to carry tensile stresses at the location of the crack; therefore, the tensile stress of reinforcing steel is more than its value in midway between two cracks where concrete resists moderate amount of tension. Hence, steel yielding initiates from a section in which the concrete is cracked, and then it propagates along its length by increasing the amount of loads. As a result, after the occurrence of the first yielding in steel, stiffness reduces gradually in the average stress–strain of the embedded steel in concrete until the whole bar yields. It has been showed that if a stress–strain curve of the bare steel reinforcement is used for analyzing behavior of reinforced concrete, the results will be considerably overestimated [24].

In this research, a trilinear stress–strain relationship, as shown in Fig. 1b, is utilized to model the reinforcing bars. The first line of this stress–strain curve has the slope of E_s, which is steel modulus of elasticity, up to a critical point corresponding to the initial yielding of steel. Then, it continues with a reduced slope until the whole reinforcement yields at the average stress of f_{yield} which is the yield stress of a bare steel bar. Then, the stress remains constant until failure. The strains corresponding to the initial yielding and yielding of the whole steel are equal to $0.8\varepsilon_{yield}$ and $4\varepsilon_{yield}$, respectively, where ε_{yield} is the yield strain of the bare steel bars.

2.1.2 Average Compressive Stress–Strain Relationship of Concrete

It is now evident that concrete in compression subjected to transverse tensile strain has less strength and stiffness than a uniaxially compressed concrete. This phenomenon is called compression softening, and it is quantified by incorporating softening coefficients into stress–strain curve of concrete [18, 37, 38]. A second-degree parabola, such as Hognestad curve [39], is widely used function for

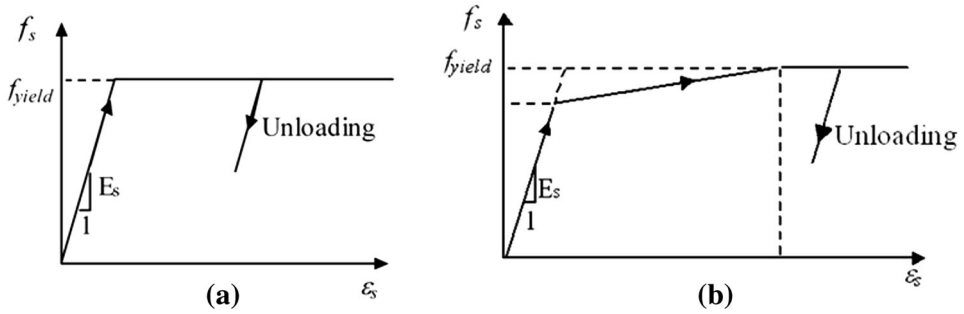

Fig. 1 **a** Bilinear behavior of steel bars; **b** proposed trilinear behavior of steel bars

ascending portion of the basic compressive stress–strain curve which is used in this study. The descending part of the curve is also a parabola limited by ε_f, which is the strain when stress falls to zero (Fig. 2). Based on Kent and Park research [40], the following relation for this strain is proposed [28]:

$$\varepsilon_f = \frac{(f_c' + 7)\varepsilon_c' - 0.042}{f_c' - 7} \quad (1)$$

where f_c' is uniaxial compressive strength of the concrete in MPa, and ε_c', which is a negative quantity, is the strain of the concrete cylinder at the point corresponding to f_c'. If psi unit is used for stresses, 7 and 0.042 should be replaced by 1000 and 6, respectively. The suggested curve for falling branch reflects the phenomenon of low strength concrete has low-slope descending portion. As shown in Fig. 2, the last part of the compression curve is assumed to be a plateau at $0.2f_c'$.

It should be noted that the employed model is calibrated for reinforced concrete specimens 890 × 890 mm^2 square with 70 mm thickness (35 inch × 35 inch × 2.75 inch) [28]. To use the constitutive laws for elements with different sizes, a localization limiter should be employed [33]. There are several kinds of localization limiters, and the simplest method which is employed in this study is crack band method, CBM [34]. CBM proposes a correlation between the element size and the constitutive laws in a way that the total fracture energy of concrete G_F remains constant. This is performed by adjusting the value of ε_f with the element size. For this purpose, the value of ε_f should be decreased by increasing the size of element. In Fig. 3, the shaded area is equal to G_f/h_0, where h_0 is the size of element (in this study 890 mm or 35 inch). Thus, for a square element with different sizes of h, the value of ε_f is modified as follows, and it is denoted by $\bar{\varepsilon}_f$:

$$\bar{\varepsilon}_f = \frac{h_0}{h}(\varepsilon_f - \varepsilon_1) + \varepsilon_1 \quad (2)$$

where ε_1 is the plastic strain corresponding to the peak point of stress–strain relation, as shown in Fig. 3.

The previous study [28] showed that maximum attainable compressive stress in concrete and its corresponding strain increase by increasing the reinforcement ratio. To consider this phenomenon in stress–strain curve of concrete, two modification factors, including α and μ, were introduced to adjust the values of f_c' and ε_c' and denoted by f_c'' and ε_c'', respectively:

$$f_c'' = \alpha f_c', \alpha = 1 + 0.03(100\rho_x)^2(100\rho_y)^2 \quad (3)$$

$$\varepsilon_c'' = \mu\varepsilon_c', \mu = 1 + 0.04(100\rho_x)^2(100\rho_y)^2 \quad (4)$$

where ρ_x and ρ_y are reinforcement ratios of the orthogonally reinforced concrete panel in x- and y-directions, respectively.

To describe the softening effect of the basic curve which was defined above, a factor proposed by Vecchio

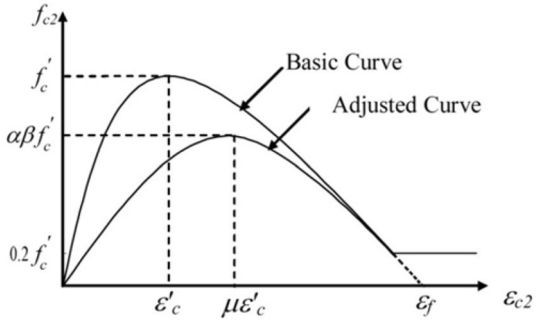

Fig. 2 Proposed compressive average stress–strain model for concrete

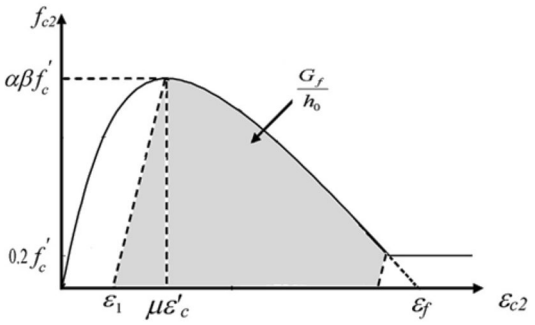

Fig. 3 Fracture energy of compressive concrete

and Collins [18] in the following form is applied to the curve to modify the maximum attainable compressive stress:

$$\beta = \frac{1}{0.8 - 0.34\varepsilon_{c1}/\varepsilon'_c} \leq 1 \tag{5}$$

in which ε_{c1} is the principal tensile strain of concrete. As a result, the compression curve of reinforced concrete panels will be obtained in the form of Fig. 2 and formulated as follows:

$$f_{c2} = \beta f''_c \left[\left(\frac{\varepsilon_{c2} - \varepsilon''_c}{\varepsilon''_c} \right)^2 - 1 \right], \frac{\varepsilon_{c2}}{\varepsilon''_c} \leq 1 \tag{6a}$$

$$f_{c2} = \beta f''_c \left[\left(\frac{\varepsilon_{c2} - \varepsilon''_c}{\varepsilon''_f - \varepsilon''_c} \right)^2 - 1 \right], \frac{\varepsilon_{c2}}{\varepsilon''_c} > 1 \tag{6b}$$

where f_{c2} and ε_{c2} represent the average principal compressive stress and strain in cracked concrete, respectively, and ε_{c1} is the coexisting tensile strain.

2.2 Average Tensile Stress–Strain Relationship of Concrete

Neglecting concrete tensile stiffness can result in significant overestimating of the post-cracking deformation in reinforced concrete structures [18]. An experimental investigation to examine the cracking behavior of reinforced concrete panels conducted by Wollrab et al. [41]. According to their work, it can be concluded that reinforcement spacing does not have a significant impact on the post-cracking contribution of concrete, while increasing the reinforcement ratio has a clear influence, and it makes the post-peak branch be steeper; as a result, the average contribution of concrete decreases. In addition, the result of their experiment showed that there are three distinct branches in tensile stress–strain curve of concrete: (1) a linearly ascending branch of uncracked concrete; (2) a crack formation phase; (3) the descending branch with stable crack pattern. According to this conceptual model, the average tensile stress–strain relation of cracked concrete is depicted in Fig. 4 and branches of this curve are formulated as follows:

$$f_{c1} = E_c \varepsilon_{c1} \quad \varepsilon_{c1} < \varepsilon_{cr} \tag{7a}$$

$$f_{c1} = f_{cr} \quad \varepsilon_{cr} < \varepsilon_{c1} < \varepsilon'_{cr} \tag{7b}$$

$$f_{c1} = \frac{f_{cr}}{1 + \sqrt{k\varepsilon_{c1}} - \sqrt{k\varepsilon'_{cr}}} \quad \varepsilon'_{cr} < \varepsilon_{c1} \tag{7c}$$

where f_{c1} represents the average tensile stress in cracked concrete; E_c is the elastic modulus of concrete in tension which can be taken as $2f'_c/\varepsilon'_c$; f_{cr} is the average tensile stress of concrete in the crack formation phase; and k is defined as follows:

$$k = 300 + 250(100\rho_x)(100\rho_y). \tag{8}$$

The previous research [28] showed that f'_c and reinforcement ratio are two parameters influencing the value of f_{cr} and the following relation in MPa was proposed:

$$f_{cr} = 0.3\alpha' \sqrt{f'_c + 8} \tag{9}$$

where α' is interestingly equal to α as defined in Eq. (3). For psi units, 0.3 and 8 should be replaced by 3.6 and 1150, respectively. In Eq. (7a, 7b, 7c), ε_{cr} is the average tensile strain at which concrete initiates cracking, and ε'_c is the strain corresponding to the end of crack formation phase. The experimental database illustrates that ε'_c has a direct relationship with the reinforcement ratio, and the following correlation is proposed for this parameter [27]:

$$\varepsilon'_{cr} = \eta\varepsilon_{cr}, \eta = 1 + 6(100\rho_x)(100\rho_y). \tag{10}$$

2.3 Nonlinear Analysis Procedure

In this study, it is aimed to apply the above-mentioned constitutive laws, obtained from the previous research based on some available test results of RC panels [28], for the analysis of RC beams. Therefore, each element in the FEM mesh is considered to be a membrane element, as shown in Fig. 5. The reinforcement and forces on each element in x- and y-directions are delineated in Fig. 5. To

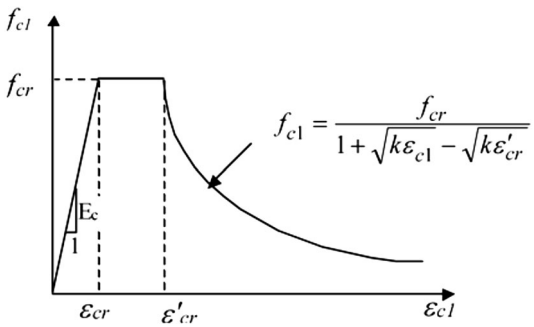

Fig. 4 Proposed tensile average stress–strain model for concrete

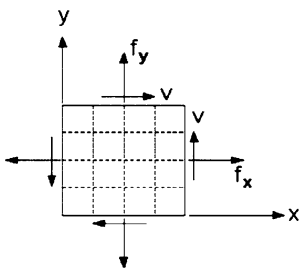

Fig. 5 FEM model of RC elements and its forces

Table 1 Cross-sectional properties of Bresler–Scordelis beams

Beam no.	*b*, mm	*h*, mm	*d*, mm	*L*, mm	Span, mm	Bott. steel	Top steel	Stirrups
OA1	310	556	461	4100	3660	4 No. 9	–	–
OA2	305	561	466	5010	4570	5 No. 9	–	–
OA3	307	556	462	6840	6400	6 No. 9	–	–
A1	307	561	466	4100	3660	4 No. 9	2 No. 4	No. 2@ 210
A2	305	559	464	5010	4570	5 No. 9	2 No. 4	No. 2@ 210
A3	307	561	466	6840	6400	6 No. 9	2 No. 4	No. 2@ 210
B1	231	556	461	4100	3660	4 No. 9	2 No. 4	No. 2@ 190
B2	229	561	466	5010	4570	4 No. 9	2 No. 4	No. 2@ 190
B3	229	556	461	6840	6400	5 No. 9	2 No. 4	No. 2@ 190
C1	155	559	464	4100	3660	2 No. 9	2 No. 4	No. 2@ 210
C2	152	559	464	5010	4570	4 No. 9	2 No. 4	No. 2@ 210
C3	155	554	459	6840	6400	4 No. 9	2 No. 4	No. 2@ 210

1 mm ≅ 0.04 inch ≅ 0.0033 ft

Table 2 Material properties of Bresler–Scordelis beams

Reinforcement				Concrete		
				Beam no.	f'_c, *MPa*	f_r, *MPa*
Bar size	No. 2	No. 4	No. 9	OA1	22.6	3.97
				OA2	23.7	4.34
Diameter, mm	6.4	12.7	28.7	OA3	37.6	4.14
				A1	24.1	3.86
Area, mm^2	32.2	127	645	A2	24.3	3.73
				A3	35.1	4.34
f_y, MPa	325	345	555	B1	24.8	3.99
				B2	23.2	3.76
f_u, MPa	430	542	933	B3	38.8	4.22
				C1	29.6	4.22
E_s, MPa	190,000	201,000	218,000	C2	23.8	3.93
				C3	35.1	3.86

1 MPa ≅ 145 psi, 1 mm ≅ 0.04 inch

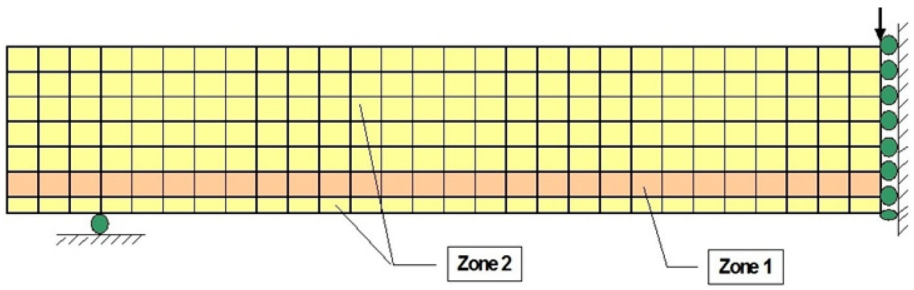

Fig. 6 FEM model of without stirrup beams of Bresler–Scordelis

construct global and local stiffness matrices of elements and the whole structure, two other sets of equations are needed: (1) compatibility equations and (2) equilibrium equations. Assuming that steel bars carry no shear stresses, the equilibrium equations can be written as follows:

$$f_x = f_{cx} + \rho_x f_{sx} \tag{11a}$$

$$f_y = f_{cy} + \rho_y f_{sy} \tag{11b}$$

where f_x and f_y are longitudinal and transverse stresses applied in the *x*- and *y*-directions, respectively; f_{cx} and f_{cy}

Table 3 Longitudinal reinforcement of no stirrup beams of Bresler–Scordelis in different zones

Beam number	Zone	
	1	2
OA1	9.19	0
OA2	11.7	0
OA3	14.2	0

are the corresponding stresses in concrete; and f_{sx} and f_{sy} are the corresponding values for reinforcement.

Assuming that there is no slip between reinforcement and concrete, the compatibility leads to the same longitudinal and transversal average strain for both steel and concrete. Another assumption considered in this model is that the principal stresses and strains have the same axes. The described constitutive laws along with equilibrium and compatibility provide a set of nonlinear equation which should be solved numerically.

2.4 Finite Element Procedure

A reinforced concrete structure, such as a beam or shear wall, under a given loading can be considered as an assemblage of some membrane elements. Thus, simultaneous solving the equilibrium, compatibility, and nonlinear constitutive laws governing all the elements yields the load-deformation response of the whole structure. Fortunately, with the current advances in the finite element methods, this task is feasible easily in an approximate manner with a desirable accuracy. An efficient FEM algorithm for the nonlinear analysis of reinforced concrete structures is suggested by Vecchio [16] which is briefly explained as follows. Based on this procedure, some modifications are made in linear elastic FEM to incorporate nonlinear constitutive laws. Therefore, the stress–strain relationships presented previously in this study can be utilized in examining nonlinear behavior of reinforced concrete structures.

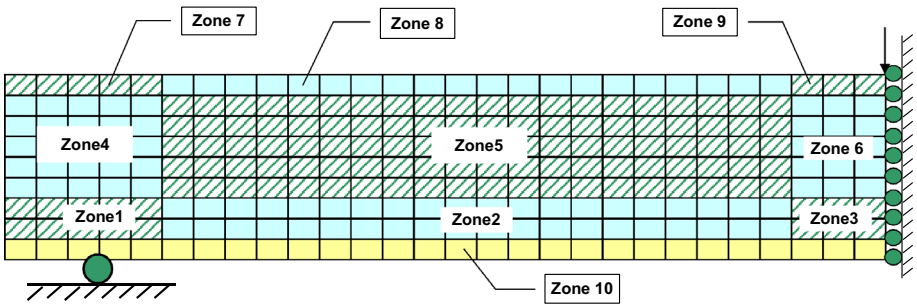

Fig. 7 FEM model of with stirrup beams of Bresler–Scordelis

Table 4 Reinforcement of with stirrup beams of Bresler–Scordelis in different zones (top: ρ_x %, bottom: ρ_y %)

Beam number	Zone									
	1	2	3	4	5	6	7	8	9	10
A1	6.43	6.43	6.43	0	0	0	2.06	2.06	2.06	0
	0.21	0.1	0.16	0.21	0.1	0.16	0.21	0.1	0.16	0
A2	5.53	5.53	5.53	0	0	0	0.83	0.83	0.83	0
	0.21	0.11	0.16	0.21	0.11	0.16	0.21	0.11	0.16	0
A3	6.6	6.6	6.6	0	0	0	0.83	0.83	0.83	0
	0.21	0.1	0.16	0.21	0.1	0.16	0.21	0.1	0.16	0
B1	8.54	8.54	8.54	0	0	0	1.1	1.1	1.1	0
	0.29	0.15	0.22	0.29	0.15	0.22	0.29	0.15	0.22	0
B2	8.62	8.62	8.62	0	0	0	1.11	1.11	1.11	0
	0.29	0.16	0.22	0.29	0.16	0.22	0.29	0.16	0.22	0
B3	10.77	10.77	10.77	0	0	0	1.11	1.11	1.11	0
	0.29	0.16	0.22	0.29	0.16	0.22	0.29	0.16	0.22	0
C1	6.37	6.37	6.37	0	0	0	1.63	1.63	1.63	0
	0.42	0.2	0.32	0.42	0.2	0.32	0.42	0.2	0.32	0
C2	12.98	12.98	12.98	0	0	0	1.67	1.67	1.67	0
	0.43	0.22	0.32	0.43	0.22	0.32	0.43	0.22	0.32	0
C3	12.73	12.73	12.73	0	0	0	1.63	1.63	1.63	0
	0.42	0.21	0.32	0.42	0.21	0.32	0.42	0.21	0.32	0

In the finite element method, material stiffness matrix [D] is employed to relate the stresses to strains:

$$\{f\} = [D]\{\varepsilon\} \tag{12}$$

where $\{f\} = \langle f_x | f_y | v_{xy} \rangle$ represents the stresses vector and $\{\varepsilon\} = \langle \varepsilon_x | \varepsilon_y | \gamma_{xy} \rangle$ is the strain vector according to plain stress theory, in which f_x and f_y are normal stresses in x- and y-directions, respectively, v_{xy} shear stress, and ε_x, ε_y, and γ_{xy} are the corresponding strains.

The material stiffness matrix is defined by combining component stiffness matrices using appropriate transformation to incorporate directional dependence of materials. According to the material model, cracked concrete element is considered as an orthotropic material with its principal axes corresponding to the direction of principal compressive and tensile strains. Moreover, the effect of Poisson's ratio can be neglected after cracking; therefore, the concrete material stiffness matrix with respect to principal axes 1 and 2 can be stated in terms of $\bar{E}_{c1} = f_{c1}/\varepsilon_{c1}$, $\bar{E}_{c2} = f_{c2}/\varepsilon_{c2}$, and $\bar{G}_c = \bar{E}_{c1}\bar{E}_{c2}/(\bar{E}_{c1} + \bar{E}_{c2})$ which are secant moduli of cracked concrete. For each reinforcing bar, the material stiffness matrix is defined in terms of $\bar{E}_{sx} = f_{sx}/\varepsilon_x$ and $\bar{E}_{sy} = f_{sy}/\varepsilon_y$ which are the secant moduli of reinforcement in x- and y-directions.

Having determined the material stiffness matrix [D], the stiffness matrix of element [k] can be evaluated as follows:

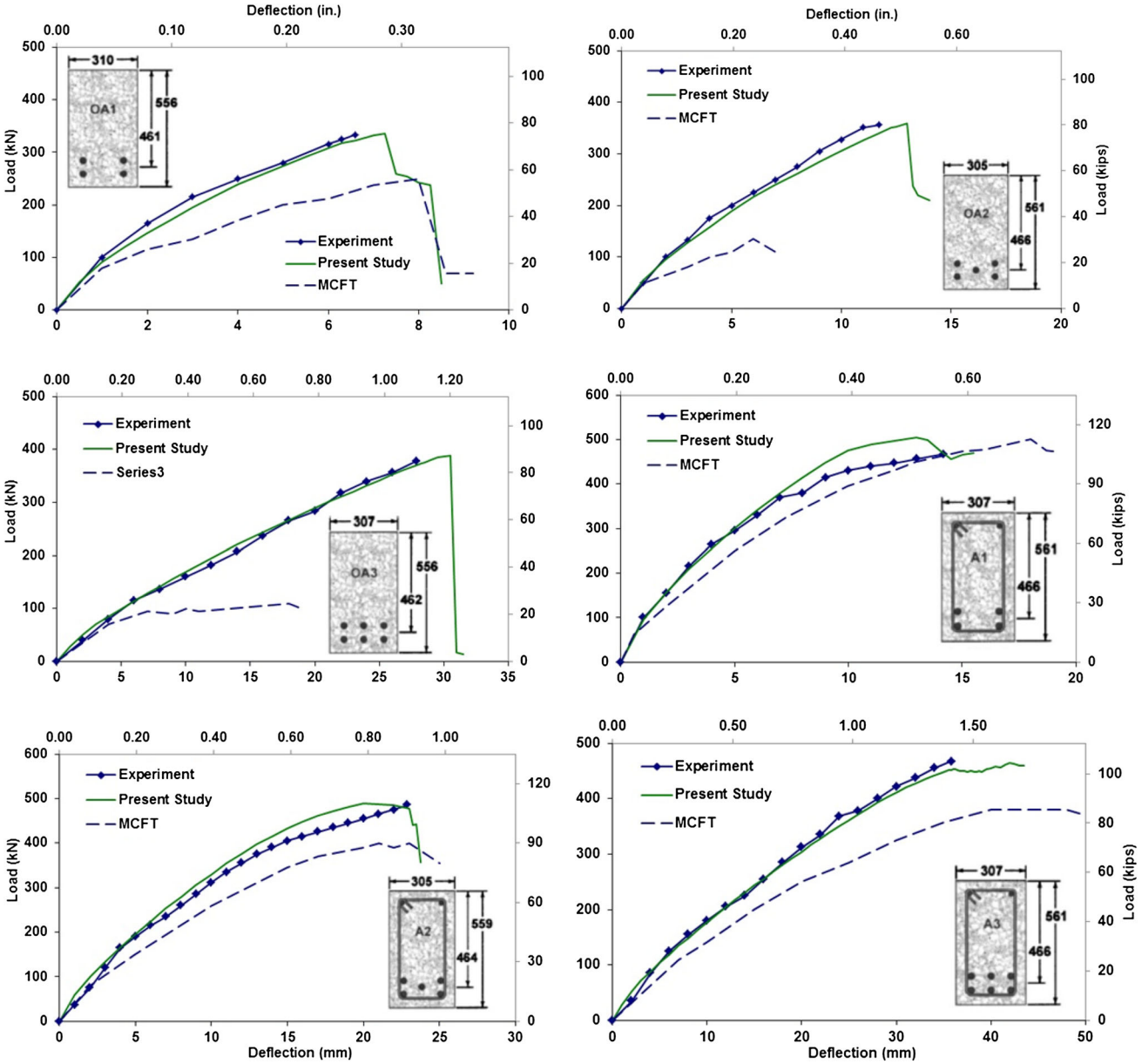

Fig. 8 Comparison of load-deformation curves of the present study, MCFT [23], and the tests [43]

$$[k] = \int [B]^T [D][B] \mathrm{d}V. \tag{13}$$

Now, the steps of a nonlinear analysis are as follows. At first, topological properties of the structure (e.g., node coordinates, element indices, support conditions, etc.) and material properties (e.g., concrete and steel stiffness matrices, reinforcement orientation, etc.) are determined. Next, nodal loads and distributed loads are input and form a nodal force vector $\{R\}$. In the next step, secant material stiffness of each material is calculated (i.e., $\bar{E}_{c1}$, $\bar{E}_{c2}$, $\bar{E}_{sx}$, and $\bar{E}_{sy}$), and $[D]$ is computed. The element stiffness matrices $[k]$ are calculated and assembled in the global stiffness matrix of the structure $[K]$. Then, the structure stiffness matrix is inverted, and joint displacements $\{r\}$ are found as follows:

$$\{r\} = [K]^{-1}\{R\}. \tag{14}$$

Using the joint displacement, the element strains and stresses can be determined as follows:

$$\{\varepsilon\} = [B]\{r\} \tag{15}$$

$$\{f\} = [D]\{\varepsilon\}. \tag{16}$$

Knowing the strains and stresses of each element, new material stiffness matrices $[D]$ are calculated, and it is used for the next iteration. This procedure is repeated until convergence is achieved.

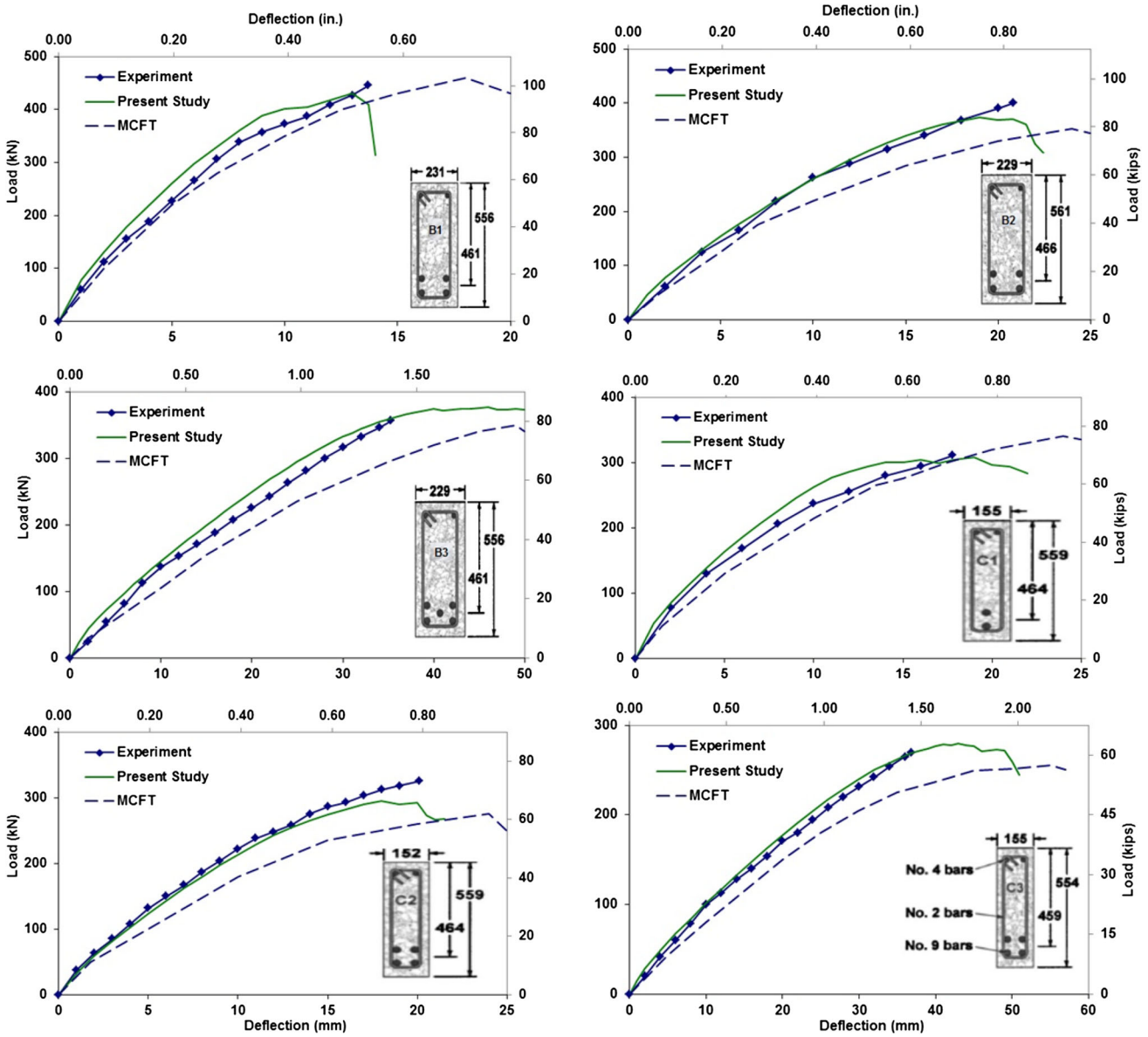

Fig. 8 continued

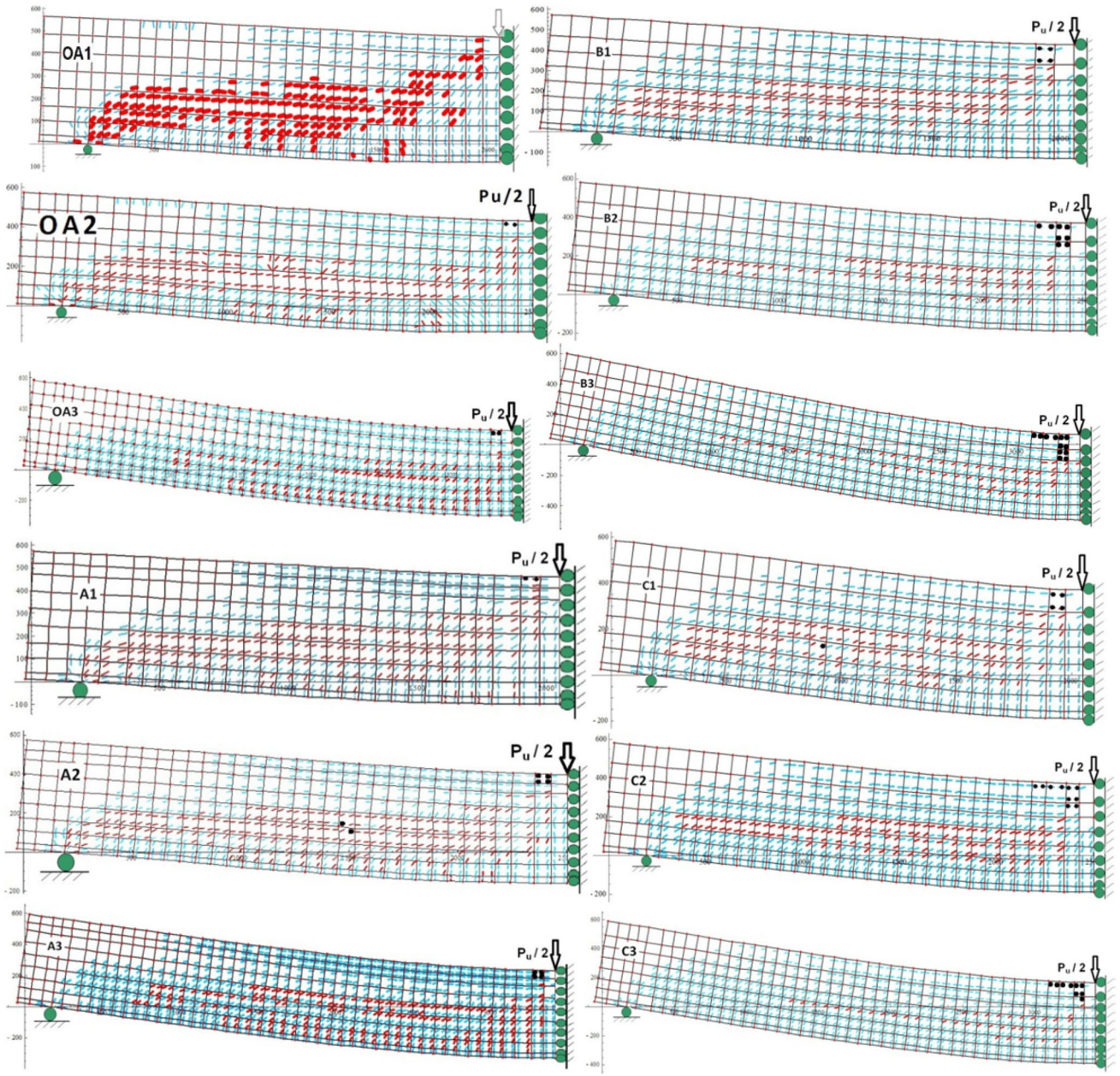

Fig. 9 Predicted crack pattern of the Bresler–Scordelis beams

3 Results and Discussion

To assess the proposed model, the results of some experimental tests on beams are compared with the present model. The test experiments conducted by Bresler and Scordelis [42] and their replicates by Vecchio and Shim [43], including a set of beams with a wide range of span-to-depth ratios and longitudinal and transversal reinforcement ratios which encompass various types of failure, are selected to evaluate the predictions of the proposed model by comparing the results.

3.1 Characteristics of Experimental Specimens

A four series of three beams tested by Bresler and Scordelis [42] named OA, A, B, and C have a different longitudinal reinforcement ratio, transverse reinforcement ratio, length of span, cross sectional size, and concrete compressive (and consequently tensile) resistance. All the beams are simply supported having a single-concentrated load at the mid-span. The span-to-depth ratios vary from 3.3 to 5.8. The ratio of shear reinforcements ranged from 0 to 0.002. Detailed properties of the beams are presented in Table 1.

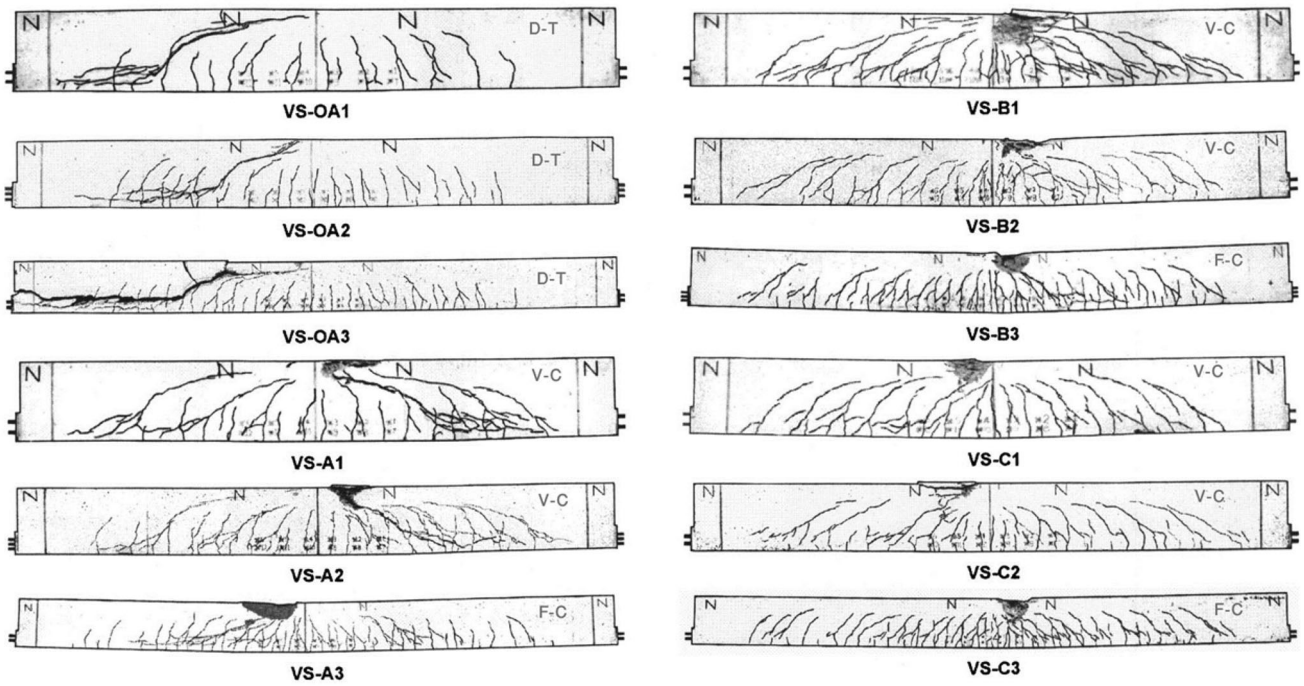

Fig. 10 Cracking pattern and failure mode for experimental tests [43] (*D-T* diagonal tension, *V-C* shear-compression, *F–C* flexure-compression)

The longitudinal reinforcements of beams are all No. 4 bars, while shear reinforcement in the form of stirrups is No. 2 bars. OA beams have no shear reinforcement. To impose the shear failure mode to the beams, all the beams are constructed with high ratios of longitudinal bars. Geometrical and mechanical properties of concrete, longitudinal bars, and transverse bars are included in Table 2. The maximum aggregate size used in the beams is 20 mm. All the beams were loaded by a monotonic load control mechanism at the mid-span.

3.2 Corroborating the Results with Experimental Database

A 2D nonlinear finite element analysis based on the discussed procedure is performed to study the load-deformation behavior and crack propagation of Bresler–Scordelis beams. Because of the symmetry of beams, only a half of beams are modeled. FEM mesh is constructed using four-node quadrilateral elements of 80 mm × 80 mm (3.15 inch × 3.15 inch). Longitudinal and transverse reinforcements are modeled in a smeared manner. Schematic view of beam models along with smeared reinforcement percent for beams without stirrups is presented in Fig. 6 and Table 3, and the ones for beams with stirrups are depicted in Fig. 7 and Table 4. The models are studied under displacement-control monotonic loading by imposing 0.5 mm (0.02 inch) displacement steps on OA and A beams and 1.0 mm (0.04 inch) steps on B and C beams.

In Fig. 8, load-deformation curves of the present study are compared with the results of the experimental tests[25] and also with the results of MCFT [28]. From this figure, it can be concluded that the proposed method predicts nonlinear behavior of the beams with an acceptable accuracy for both beams with and without stirrups.

To delineate the fracture mode of the beams, a graphical ability is added to the FEM code which shows the shear-critical cracks in a different color seen darker in Fig. 9. In addition, the Gaussian points at which compressive failure occurs are shown by bold points. According to Fig. 9, the predicted cracking patterns and failure modes of the beams are in a good agreement with the experimental test results, as shown in Fig. 10.

In Table 5, the ultimate loads, P_u, of the present study are compared with those of the experimental tests, MCFT [23] and DSFM [20–22]. DSFM is a newer version of MCFT aiming to reduce the deficiency of MCFT in predicting load-deformation behavior of RC beams with low stirrups or without stirrups. According to Table 5, the ratio of prediction to experimental ultimate loads has a mean of 1.02 and covariance of 5 % for the proposed method, while these values for DSFM approach are 1.15 and 11 %, and for MCFT, they are 1.42 and 55 %, respectively. As seen in Table 5, the strength of beams containing no stirrups is significantly underestimated by MCFT.

In Table 6, computational results for the mid-span displacements at peak load, δ_0, of the present study are compared with those of the experimental tests, MCFT and

DSFM. According to this table, the ratio of prediction to experimental ultimate displacements has a mean of 0.98 and covariance of 9 % for the proposed method, while these values for MCFT are 0.97 and 40 % and for DSFM approach are 0.95 and 24 %, respectively.

4 Conclusions

Recently developed interactive constitutive laws for normal strength concrete and reinforcing steel were integrated with a nonlinear finite element procedure to predict the shear behavior of reinforced concrete structures. The constitutive laws were used to obtain the secant stiffness of elements which is needed for nonlinear analysis. Conclusions derived from the present work can be summarized as follows:

1. Interactive effects of concrete and reinforcing bars on the average stress–strain relations of each other are an important phenomenon that must be considered in constitutive laws.
2. The response of shear-critical reinforced concrete beams with or without stirrups can be predicted with

Table 5 Ultimate load obtained by the present study, MCFT [23], DSFM [43], and the tests [43]

Beam number	P_u, kN				$P_{u\text{-test}}/P_{u\text{-calc}}$		
	Test	Present study	MCFT	DSFM	Present study	MCFT	DSFM
OA1	334	348	250	316	096	1.34	1.06
OA2	356	333	135	270	1.07	2.64	1.32
OA3	378	344	110	294	1.10	3.44	1.29
A1	467	509	500	472	0.92	0.93	0.99
A2	489	499	400	399	0.98	1.22	1.23
A3	467	456	380	366	1.02	1.23	1.28
B1	445	432	460	423	1.03	0.97	1.05
B2	400	376	352	327	1.06	1.14	1.22
B3	356	371	350	355	0.96	1.02	1.00
C1	311	304	340	307	1.02	0.91	1.01
C2	325	296	275	258	1.10	1.18	1.26
C3	269	271	255	255	0.99	1.05	1.05
				Mean	1.02	1.42	1.15
				C.o.V %	6	55	11

1 kN ≅ 0.225 kips

Table 6 Mid-span deflection at peak load obtained by the present study, MCFT [23], DSFM [43], and the tests [43]

Beam number	δ_0, mm				$\delta_{0-\text{test}}/\delta_{0-\text{calc}}$		
	Test	Present study	MCFT	DSFM	Present study	MCFT	DSFM
OA1	6.6	7.75	8	12.0	0.85	0.80	0.55
OA2	11.7	11.7	6	18.5	1.00	1.95	0.63
OA3	27.9	26.0	18	20.8	1.07	1.55	1.34
A1	14.2	14.0	18	15.8	1.01	0.79	0.90
A2	22.6	21.0	21	19.5	1.08	1.08	1.16
A3	35.8	38.0	40	44.6	0.94	0.90	0.80
B1	13.7	13.0	18	15.3	1.05	0.76	0.90
B2	20.8	19.0	24	19.5	1.09	0.87	1.07
B3	35.3	40.0	49	39.0	0.88	0.72	0.91
C1	17.8	17.0	24	18.3	1.05	0.74	0.97
C2	20.1	20.0	24	17.3	1.01	0.84	1.16
C3	36.8	37.5	55	36.3	0.98	0.67	1.01
				Mean	1.00	0.97	0.95
				C.o.V %	8	40	24

1 mm ≅ 0.04 inch

a good accuracy using the proposed interactive constitutive laws.

3. The nonlinear finite element formulation based on secant-stiffness approach can provide acceptable results, and low-order elements can be used for the analysis which makes the procedure very efficient and simple.
4. Corroboration with experimental data, including shear-critical beams with a wide range of properties, showed that the model can predict the cracking patterns, shear capacity, load-deformation response, and failure mode with an excellent agreement with reality.
5. The accuracy of response prediction based on the interactive constitutive laws is more than MCFT and DSFM when they are compared with the experimental test results.

References

1. Joint ASCE-ACI Committee 445 (1998) Recent approaches to shear design of structural concrete. J Struct Eng ASCE 124 (12):1375–1417
2. CEB (1997) Concrete Tension and Size Effect, Contribution from CEB Task Group 2.7, Comité Euro-International du Béton, Lausanne, Switzerland
3. Lucas W, Oehlers DJ, Ali M (2011) Formulation of a shear resistance mechanism for inclined cracks in RC beams. J Struct Eng ASCE 137(12):1480–1488
4. Arslan G (2008) Cracking shear strength of RC slender beams without stirrups. J Civil Eng Manage 14(3):177–182
5. Pérez Caldentey A, Padilla P, Muttoni A, Fernández RM (2012) Effect of load distribution and variable depth on shear resistance of slender beams without stirrups. ACI Struct J 109(5):595–603
6. Keskin RS, Arslan G (2013) Predicting diagonal cracking strength of rc slender beams without stirrups using ANNs. Comp Conc 12(5):697–715
7. Jeong JP, Kim W (2014) Shear resistant mechanism into base components: beam action and arch action in shear-critical RC members. Int J Conc Struct Mater 8(1):1–14
8. Fernández RM, Muttoni A, Sagaseta J (2015) Shear strength of concrete members without transverse reinforcement: a mechanical approach to consistently account for size and strain effects. Eng Struct 99:360–372
9. Cavagnis F, Ruiz MF, Muttoni A (2015) Shear failures in reinforced concrete members without transverse reinforcement: an analysis of the critical shear crack development on the basis of test results. Eng Struct 113:157–173
10. Kazemi MT, Broujerdian V (2006) Reinforced concrete beams without stirrups considering shear friction and fracture mechanics. Can J Civ Eng 33:161–168
11. Kazemi MT, Broujerdian V (2006) Discussion of repeating a classic set of experiments on size effect in shear of membranes without stirrups, by Bentz EC and Buckley S. ACI Struct J 103(5):754–755
12. Bazant ZP, Kazemi MT (1991) Size effect on diagonal shear failure of beams without stirrups. ACI Struct J 88(3):268–276
13. Bažant ZP, Yu Q (2005) Designing against size effect on shear strength of reinforced concrete beams without stirrups: I-formulation. J Struct Eng ASCE 131(12):1855–1877
14. Bažant ZP, Yu Q (2005) Designing against size effect on shear strength of reinforced concrete beams without stirrups: II-verification. J Struct Eng ASCE 131(12):1886–1897
15. Xu S, Zhang X, Reinhardt HW (2012) Shear capacity prediction of reinforced concrete beams without stirrups using fracture mechanics approach. ACI Struct J 109(5):705–714
16. Gastebled OJ, May IM (2001) Fracture mechanics model applied to shear failure of reinforced concrete beams without stirrups. ACI Struct J 98(2):184–190
17. Collins MP (1978) Towards a rational theory for RC members in shear. J Struct Eng ASCE 104(4):649–666
18. Vecchio FJ, Collins MP (1986) The modified compression-field theory for reinforced concrete elements subjected to shear. ACI J Proceed 83(2):219–231
19. Vecchio FJ (1989) Nonlinear finite element analysis of reinforced concrete membranes. ACI Structural Journal 86(1):26–35
20. Vecchio FJ (2000) Disturbed stress field model for reinforced concrete: formulation. J Struct Eng ASCE 126(8):1070–1077
21. Vecchio FJ (2001) Disturbed stress field model for reinforced concrete: implementation. J Struct Eng ASCE 127(1):12–20
22. Vecchio FJ, Lai D, Shim W, Ng J (2001) Disturbed stress field model for reinforced concrete: validation. J Struct Eng ASCE 127(4):350–358
23. Vecchio FJ (2000) Analysis of shear-critical reinforced concrete beams. ACI Struct J 97(1):102–110
24. Hsu TTC, Zhang LX (1997) Nonlinear analysis of membrane elements by fixed-angle softened-truss model. ACI Struct J 94(5):483–492
25. Dabbagh H, Foster SJ (2006) A smeared-fixed crack model for FE analysis of RC membranes incorporating aggregate interlock. Adv Struct Eng 9(1):91–102
26. Bhatt P, Kader MA (1998) Prediction of shear strength of reinforced concrete beams by nonlinear finite element analysis. Comput Struct 68(1):139–155
27. Lee J, Kim SW, Mansour M (2011) Nonlinear analysis of shear-critical reinforced concrete beams using fixed angle theory. J Struct Eng ASCE 137(10):1017–1029
28. Broujerdian V, Kazemi MT (2010) Smeared rotating crack model for reinforced concrete membrane elements. ACI Struct J 107(4):411–418
29. Ayoub A, Flippou FC (1998) Nonlinear finite element analysis of reinforced concrete shear panels and walls. J Struct Eng ASCE 124(3):298–308
30. Sadeghi K (2014) Analytical stress-strain model and damage index for confined and unconfined concretes to simulate RC structures under cyclic loading. Int J Civil Eng 12(3):333–343
31. Arslan G, Hacisalihoglu M, Balci M, Borekci M (2014) An investigation on seismic design indicators of RC columns using finite element analyses. Int J Civil Eng 12(2):237–243
32. ACI Committee 446 (1991) Fracture mechanics of concrete: concepts, models and determination of material properties. ACI 446.1R-91, ACI, Detroit
33. ACI Committee 446 (1997) Finite Element Analysis of Fracture in Concrete Structures, ACI Committee 446 Report, American Concrete Institute, Farmington Hills, Mich
34. Bazant ZP, Oh BH (1983) Crack band theory for fracture of concrete. Matériaux et Constr 16(3):155–177
35. Prasad MVKV, Krishnamoorthy CS (2002) Computational model for discrete crack growth in plain and reinforced concrete. Comp Methods Appl Mech Eng 191(25):2699–2725
36. Slobbe AT, Hendriks MAN, Rots JG (2014) Smoothing the propagation of smeared cracks. Eng Fract Mech 132:147–168
37. Hsu TTC, Zhang LX (1996) Tension softening in reinforced concrete membrane elements. ACI Struct J 93(1):108–115
38. Belarbi A, Hsu TTC (1995) Compressive laws of softened concrete in biaxial tension-compression. ACI Struct J 92(5):562–573

39. Hognestad E (1951) Study of combined bending and axial load in reinforced concrete members, bulletin series No. 399, University of Illinois Engineering Experimental Section
40. Kent DC, Park R (1971) Flexural members with confined concrete. J Struct Div ASCE 97(7):1969–1990
41. Wollrab E, Kulkarni SM, Ouyang C, Shah SP (1996) Response of reinforced concrete panels under uniaxial tension. ACI Struct J 93(6):648–657
42. Bresler B, Scordelis AC (1963) Shear strength of reinforced concrete beams. ACI J 60(1):51–74
43. Vecchio FJ, Shim W (2004) Experimental and analytical reexamination of classic concrete beam tests. ASCE J Struct Eng 130(3):460–469